Supporting Information: Diamond Micro-Chip for Quantum Microscopy

Shahidul Asif [1], Hang Chen [2*], Johannes Cremer [3,4], Shantam Ravan [3,4,5], Jeyson Támara-Isaza [2, 3,6], Saurabh Lamsal[2], Reza Ebadi [3,5], Yan Li [1], Ling-Jie Zhou [7], Cui-Zu Chang [7], John Q. Xiao [2], Amir Yacoby [4,8], Ronald L. Walsworth [3,5,9#], Mark J.H. Ku [1,2#]*

1. Department of Materials Science and Engineering, University of Delaware, Newark, DE 19716, USA

2. Department of Physics and Astronomy, University of Delaware, Newark, DE 19716, USA

3. Quantum Technology Center, University of Maryland, College Park, MD 20742, USA

4. Department of Physics, Harvard University, Cambridge, MA 02138, USA

5. Department of Physics, University of Maryland, College Park, MD 20742, USA

6. Departamento de Física, Universidad Nacional de Colombia, 110911, Bogotá, Colombia

7. Department of Physics, Pennsylvania State University, University Park, Pennsylvania 16802, USA

8. John A. Paulson School of Applied Sciences and Engineering, Harvard University, Cambridge Massachusetts 02138, USA

9. Department of Electrical and Computer Engineering, University of Maryland, College Park, MD 20742, USA

*Equal contribution, # corresponding authors

Section 1. Robustness of DMC-sample interface

Once a DMC is properly placed on a sample, the sample can be transported between different locations and the DMC remains in place without being disturbed. A DMC also remain in its place after a wire bonding process. We note that it is generally necessary to deposit the DMC first before wire bonding, as the bonding wires will be in the way for the diamond sample containing DMC array to approach the sample of interest. Likewise, polymer-assisted transfer should generally take place prior to wire bonding. Lastly, we note that DMCs can also be held against gravity even without specialized surface preparation or adhesive material such as employed in Refs. [1,2]. For example, we have shown that with DMCs deposited on YIG or quartz substrates, when we flip the substrate over (e.g., in a measurement setup where the sample has to face down), the DMCs remain on the sample.

Section 2. Experimental setup.

The setup for wide-field microscopy of strain (Figure. 2 of the main text) and stray magnetic field (Figure. 4c of the main text) is described previously [3,4]. A 532 nm laser (Coherent Verdi 2G) provides excitation. The light is sent through a Kohler-illumination system consisting of a beam expansion lens and a 0.9 NA air objective, which expands the beam to illuminate an area of up to ~ 50×50 μm^2 on the sample. NV photoluminescence (PL) is collected by the same

objective. The collected light is separated from the excitation via a 552 nm edge dichroic (Semrock LM01-552-25). Note that the beam expansion lens is located between the laser and the dichroic; the collected light does not pass through this lens. After the dichroic, another 570 nm long-pass filter (Semrock BLP01-647R-25) further removes light not in the PL wavelength range. The collected light is imaged via a tube lens (focal length f = 200 mm) onto a CMOS camera (Basler acA1920-155um). 2 × 2 binning is applied during data analysis, and each pixel corresponds to 140 nm on the sample. A microwave (MW) signal is sourced by a signal generator (Stanford Research Systems SG384 or Windfreak USB3) and an amplifier (Minicircuits ZHL-16W-43-S+). The sample is fixed on a printed circuit board (PCB) with a co-planar waveguide (CPW). The sample substrate has a stripline that is wirebonded to the CPW of the PCB, to which MW is delivered. The MW circuits ends with an MW terminator. For stray-field microscopy, the CPW also serves to provide the electrical connection between the phantom wire and the current source. The sample and the PCB are mounted on a combined manual translation stage and piezo positioner (Thorlabs NanoMax or PhysikInstrumente P-615.3CD NanoCube XYZ Piezo System). A permanent magnet mounted on a three-axes translational stage is used to provide an external bias magnetic field. Generally, the magnet is placed right beneath the sample to provide a vertical field aligned with (111)-oriented NVs.

The same system is modified as described below for pulsed measurements (spin echo and spin relaxation in Figure. 3 of the main text). Excitation light is modulated with an acousto-optical modulator (AOM) powered by a radiofrequency (RF) driver (Gouch & Housego AOMO 3250-220 532nm and AODR 1250AFP-AD-6.6). Beam expansion light is removed so the excitation is focused onto a tight spot on the sample. The collected PL, instead of going through a tube lens and then imaged onto a camera, is directed into a single-mode fiber for confocal microscopy.

The PL is finally detected by a single photon counting module (Excelitas 28252). Photon counting is performed with a Data Acquisition System (National Instrument USB-6361, X Series DAQ Device with BNC Termination). A MW signal is supplied by Stanford Research Systems SG384 with built-in IQ control, and modulated with a switch. The NV interrogation pulse sequence is generated by a Swabian Instrument Pulse Streamer 8/2.

Section 3. Strain and stray-field microscopy.

Wide-field microscopy is performed following the technique described in Refs. [3–7]. We align an external bias magnetic field with (111)-oriented NVs. We perform optically-detected magnetic resonance (ODMR) measurements by continuously illuminating the NVs with the excitation light while driving the NVs with an MW field. The MW frequency ν is swept, and an ODMR image is captured at each MW frequency. To improve the signal-to-noise ratio (SNR), this sequence is repeated multiple times to create a set of images $PL_{i,\nu}(x,y)$. We perform post-measurement alignment of images to counteract the effect of drift [3], before summing the images at a given ν to create a signal-averaged image $PL_{\nu}(x,y)$. Then, at a given pixel (x,y), we create an ODMR spectrum PL vs ν, and fit the spectrum to extract the resonance position. This procedure is performed to extract a spatial map of both the upper and lower NV resonances, $\nu_{\pm}(x,y)$, corresponding to the the $m_s = 0 \leftrightarrow \pm 1$ transitions.

A simplified Hamiltonian for the NV electronic spin (assuming (111)-orientation) is

$$H = \left(D_g + M_z\right)S_z^2 + \gamma_e \mathbf{B} \cdot \mathbf{S},$$

where D_g=2.87 GHz is the ground-state zero-field splitting, M_z is the component of the effective electric field associated with strain (which we will call effective strain field) coupling to the S_z^2 term, γ_e=28 GHz/T is the NV gyromagnetic ratio, **B** is the net magnetic field applied to the NV, and **S**=(S_x, S_y, S_z) is the S=1 spin operator. Here, the z-axis corresponds to the quantization axis set by the nitrogen and vacancy, which is also the vertical axis for (111)-oriented NVs. In writing down this Hamiltonian, we ignore higher-order contributions from strain, which are negligible in the context of magnetometry. To leading order, the spin resonance corresponding to the $m_s = 0 \leftrightarrow \pm 1$ transitions are $\nu_\pm = D \pm \gamma_e B_z + 3\gamma_e^2 B_\perp^2/(2D)$, where we have defined the effective zero-field splitting (ZFS) $D \equiv D_g + M_Z$ and $B_\perp$ is the off-axis field.

For strain microscopy (Figure. 2), we obtain the spatial map of effective zero-field splitting $D \equiv D_g + M_z$ by extracting the common-mode shift, $D(x,y)=[\nu_+(x,y)+\nu_-(x,y)]/2$. Note that because we have aligned the external magnetic bias field with the (111)-oriented NVs and there is no stray-field present, the magnetic field is completely aligned with (111)-oriented NVs and there is no contribution from an off-axis field $B_\perp$. The effective strain field is then $M_z(x,y)= D(x,y)- D_g$, where D_g =2.87 GHz.

Due to a diamond's high index of refraction, significant NV PL undergoes total internal refraction and exits the diamond at the edges. Hence, edges are generally brighter and often saturate the corresponding camera pixels. Furthermore, PL emitted near the edges contains information from other parts of the diamond. Hence in Figure. 2, we filter out pixels within 1 μm of the edges as well as pixels with PL level exceeding a threshold value.

For magnetic microscopy (Figure. 4c), we look at the differential shift, $\Delta\nu=[\nu_+(x,y)-\nu_-(x,y)]/2$, which is then converted to magnetic field via $B_z=\Delta\nu/\gamma_e$. While the stray-field from a current-carrying wire has an off-axis component in general, the leading-order contribution from the off-axis field to $\nu_\pm$ is $\sim B_\perp^2$ and therefore contributes to the common-mode shift but not the differential shift.

Section 4. Dark Matter Detection

One proposal for the directional detection of weakly interacting massive particles (WIMPs), a dark matter (DM) candidate, is via measurement of strain tracks in diamond left by WIMPs [8]. In this multi-stage proposal, a large number of diamond crystals of ~mm^3 volume are stored in a facility (e.g., deep underground) to interact with WIMPs that pass through the diamond detector (Figure. S1). Occasionally, a WIMP, or background particle such as a neutrino, initiates a nuclear recoil cascade via collision with a carbon nucleus and damages the diamond crystal lattice; the event is first registered and triangulated by photon, phonon, or charge-carrier collection (Figure. S1a). The diamond crystal in which the event is registered is isolated, and one then uses optical and/or x-ray techniques in to look for the associated strain feature, which needs to be eventually located with nm-resolution. The strategy would be to first perform-wide-field strain microscopy to locate the strain feature with μm or sub-μm precision (Figure. S1b), and at last perform microscopy with a super-resolution technique to achieve nm-resolution (Figure. S1c). To accomplish this goal, the diamond will need to be thinned down to avoid aberration;

hence, the DMC we study here provides a representation of the eventual diamond sample for WIMP

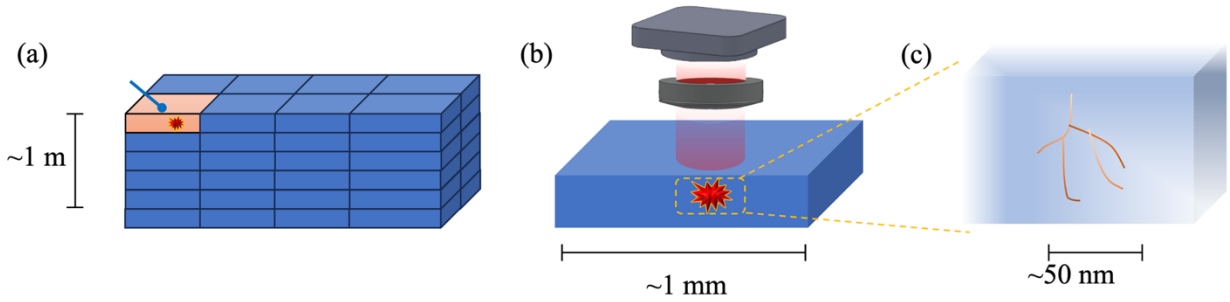


Figure S1. Schematics of directional WIMP detection. (a) An event is registered and the particular ~mm^3 volume of diamond crystal is identified for further measurement. (b) The registered diamond segment is taken for diffraction-limited microscopy, localizing the nuclear recoil track to a precision better than μm. (c) Finally, microscopy with ~nm resolution (e.g., via optical superresolution or x-ray techniques) is employed to measure the recoil track to nm precision. The incoming direction of the particle that created the nuclear recoil track can then be determined, potentially allowing discrimination of possible WIMPs from other background signals, such as from neutrinos.

detection. An important feasibility question is whether the process of thinning down diamond may introduce strain features that mask the signal of a WIMP. Ref. [8] has shown that the expected fractional strain signal from WIMPs is ~10^{-6}; the standard deviation of strain measured in this work is ~1-3×10^{-6}, comparable to the state-of-the-art in Ref. [8] (before high-pass filtering) and the expected WIMP signal. Hence, our results show that it is possible to fabricate small diamond structure and be able to maintain low strain variation profile to retain sensitivity to WIMPs.

Section 5. Spatial resolution

Spatial resolution in optical microscopy is given by the associated point spread function (PSF). The PSF is given by the Airy pattern which has the form $\mathrm{PSF}_{\mathrm{Airy}}(u)=(2J_1(u)/u)^2$, where u is some dimensionless spatial scale and J_1 is the Bessel function of the first kind of order one. The first zero occurs at $u = 3.8317 \approx 4$; the length scale corresponding to this u is the resolution according to the Rayleigh criterion. It is generally more convenient to use a Gaussian profile to approximate the PSF. The Airy pattern, to leading order in u, is $\mathrm{PSF}_{\mathrm{Airy}} = 1 - u^2/4 + O(u^4)$. A Gaussian profile of the form $\exp(-u^2/4)$ has the same expansion. Therefore, the following is a suitable Gaussian PSF:

$$\mathrm{PSF}(x,y)= \frac{1}{\pi\sigma^2} e^{-(x^2+y^2)/\sigma^2}$$

and we identify 2σ as the spatial resolution.

In Figure. 4d, we fit the two neighboring strain features to a Gaussian profile. The underlying strain features (before being broadened by optical diffraction) may not necessarily be symmetrical. To account for such asymmetry, we fit each feature to the form

$$M_z(x,y)= Ae^{-(x^2/\sigma_x^2+y^2/\sigma_y^2)}$$

The larger strain feature has a significant aspect ratio, while the difference in σ_x and σ_y is within the error bar for the small feature. We take the smaller of σ_x and σ_y of the small feature, and from it extract a spatial resolution of 450(30) nm.

The diffraction-limited resolution from the Rayleigh criterion expected for an imaging system is $\sigma=0.61\lambda/NA$, where λ is the wavelength and NA is the numerical aperture of the objective. With a 0.9 NA objective and using $\lambda=650$ nm as the typical wavelength for NV PL, we have $\sigma=440$ nm, consistent with the experimentally extracted resolution.

Section 6. Polymer-assisted dry-transfer

The polymer-assisted DMC pickup and drop-off process is accomplished on a homemade deposition apparatus as shown in Figure. 1(b). With the diamond sample held on the translational stage on the left-hand-side, we first break a DMC off from the diamond with a sharp tip mounted on the motorized translational stage on the right-hand-side. The distance between the diamond and the sample surface is kept as small as possible by adjusting the tilt stage, which eliminates the chance of the DMC flipping upside down during the landing process. Figure. 5 (a)-(e) demonstrates the schematic of picking up a DMC and transferring it onto a target sample. A micro-structure of polymer made of 0.7 μm thick photoresist LOR5A/AZ-1512 is patterned on a transparent thin glass as shown in Figure. 5 (f). The polymer is located near the corner of the glass edges, which allows us to make sufficient contact of the polymer to the DMC by slightly tilting the glass substrate. A 50 μm DMC is successfully picked up by the polymer as recorded in Figure. 5(d)-(i), where the images focus on the DMC before and after it has been picked-up.

Then the glass is moved to a location above the sample of interest. The sample shown in Figure. 5(j) is a patterned Hall bar structure of RuO_2 with four leads made of 2 nm Ti/100 nm Au. The DMC is vertically aligned to the sample location and gradually lowered down until it touches the Au leads as shown in Figure. 5(j)-(k). The tilt action and adhesion to the Au surface allows the release of the DMC from the polymer to the targeted sample in Figure. 5(k). Furthermore, with a subsequent operation shown in Figure. 5(l), we can also slightly manipulate the DMC to a desired location or orientation using a sharp tip.

Here we discuss differences between our technique and another recently reported dry-transfer technique using PMMA-PDMS stamp [9]. First, our technique does not require thermal-assistance, which is desirable for a temperature or air sensitive material, e.g,. van der Waals magnetic materials. Second, the technique in Ref [9] involves a PMMA layer that covers the whole diamond chip after the chip deposition. Thus, additionally opening a window in PMMA layer by electron-beam lithography is needed. In our work, the DMC is directly dropped off on the sample, and no additional fabrication process is needed. Lastly, since our technique does not have a layer of PMMA that holds down the chip, and thus we can recycle the chips.

We also note that Refs. [1,2] developed similar transfer technique for diamond membranes (thickness ~100 nm with lateral dimension ~100 μm). Difference between these works and our result are as follows: 1) we demonstrate the transfer of significantly smaller structures, with lateral dimension as small as 10 μm; and 2) our result does not require specialized surface preparation such as the use of polymer adhesion layer [1] (our technique can make use of it but does not require it), plasma treatment, or annealing [2], which can place limitations on the type of sample one can interface with a DMC.

As shown in Figure. 5, the use of a patterned polymer micro-structure enables us to pick up a specifically targeted chip without affecting other chips in the neighborhood. This enables a high-throughput and highly-efficient process for deploying DMCs. One can first detach many (or even all) DMCs onto a substrate (Figure. S2a). Then, each chip can be subsequently picked up for deposition (Figure. S2b). The advantage of this process is two-fold. First, detachment can be done

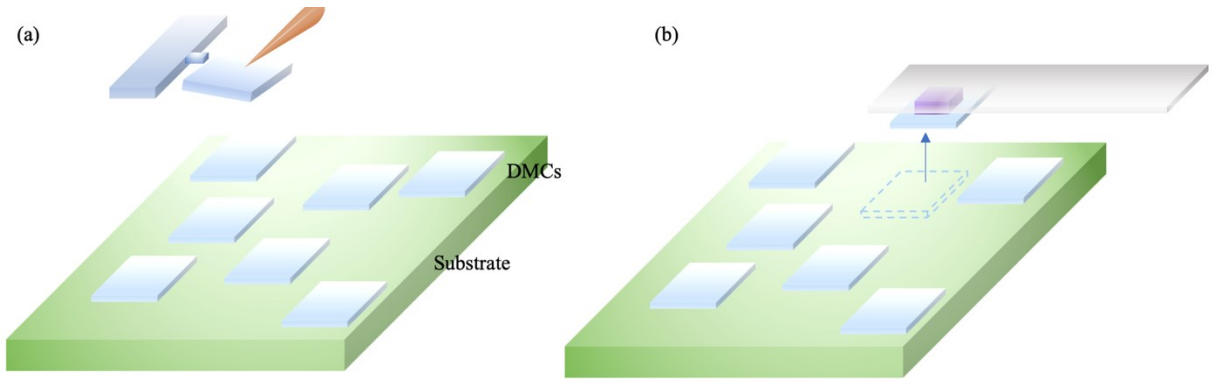
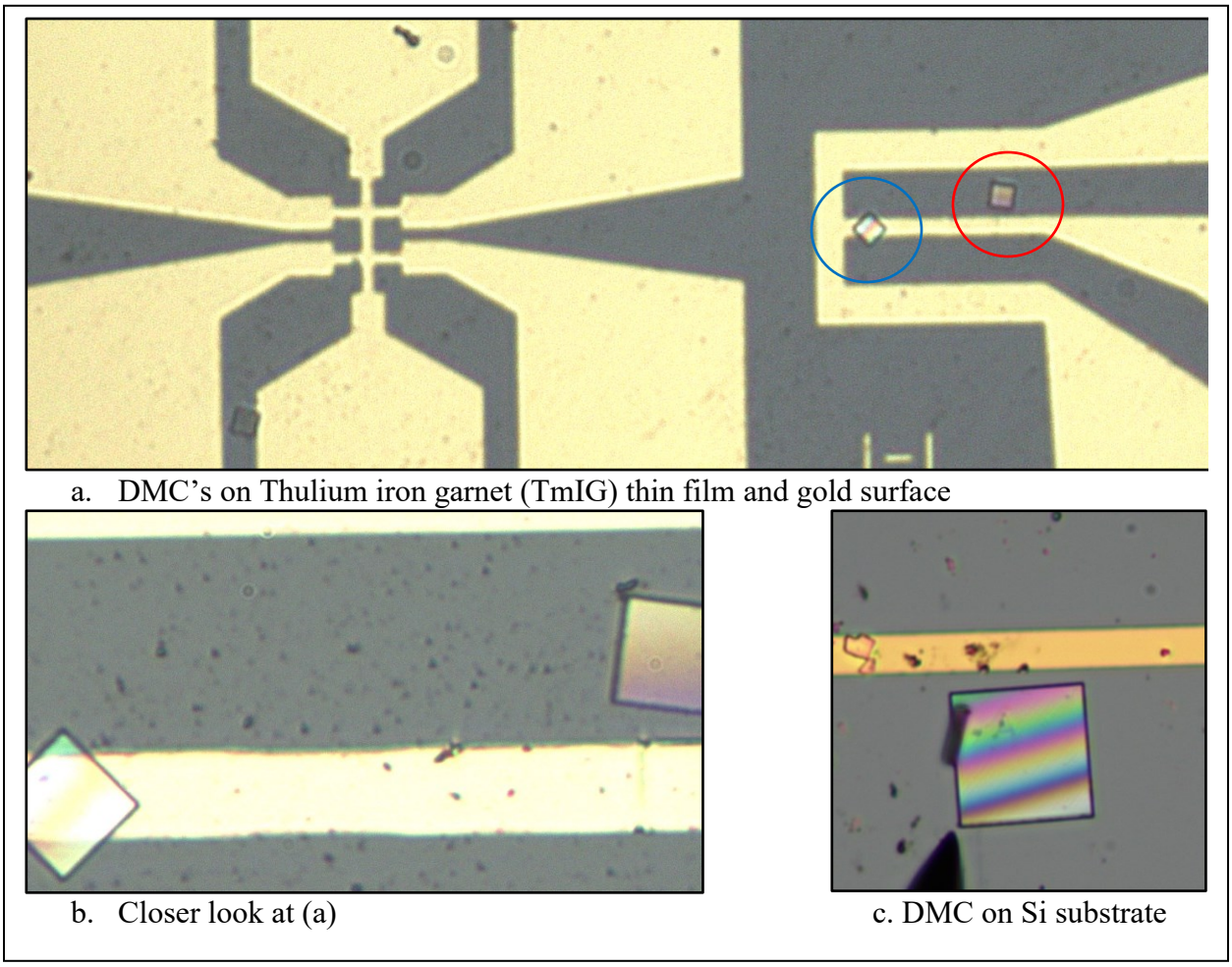


Figure S2. Instead of detaching and then depositing a DMC one at a time, our approach allows one to take advantage of the targeted-pickup capability of the polymer-assisted transfer technique to enable a high-throughput transfer process. (a) One can first detach many DMCs onto a substrate, and subsequently (b) pick up an individual DMC to transfer onto the target sample.

just once, instead of having to be done each time a chip is to be positioned, enabling greater efficiency. Second, this allows one to have chips detached and stored on a substrate, instead of remaining attached on the mainframe. The latter is risky for storage and transportation because chips can be easily detached with accident in handling; and if a chip is not detached in a controlled manner, it most likely cannot be retrieved. Hence, detaching many chips on a

substrate for storage allows one to safely store the chips for transportation and handling; and can reduce costs associated with having to fabricate DMCs again due to an accident.

Section 7: additional examples of polymer-assisted trans*fer*



a. DMC's on Thulium iron garnet (TmIG) thin film and gold surface

b. Closer look at (a)

c. DMC on Si substrate

Figure S3. (a) Successfully deposited Diamond microchip (DMC) on gold surface (blue circle) and Thulium iron garnet (TmIG) thin film (red circle); (b) closer look at the deposited DMCs in the image (a), left is on gold surface, the right is on the TmIG thin film; (c) Successfully deposited Diamond microchip (DMC) on Silicon substrate.

We have demonstrated that the transfer technique presented here is based on tilting and control and is independent of thermal control. A relevant question may come up with this is if this is a

technique that is dependent or limited to on the materials involved in the process (that is if it is applicable to only the materials those are mentioned before) or is it applicable to a broad range of materials. While developing this technique, we have also tried this method of chip dropping and deposition on two other materials along with the gold surface. We successfully deposited the diamond microchips on thin Thulium iron garnet (TmIG) thin films as well as Silicon substrates. These two materials, as well as the permalloy spin-torque device material presented in Fig. 5p (main manuscript), are not adhesive as Au surface. Hence, while this list may not be sufficient for commenting the technique as a universally applicable one that can be used for any surface, the fact that we can successfully transfer chips to these substrates, it demonstrates that the transfer technique should be generally applicable to a large range of materials.

References

(1) Guo, X.; Delegan, N.; Karsch, J. C.; Li, Z.; Liu, T.; Shreiner, R.; Butcher, A.; Awschalom, D. D.; Heremans, F. J.; High, A. A. Tunable and Transferable Diamond Membranes for Integrated Quantum Technologies. *Nano Lett.* **2021**, *21* (24), 10392–10399. https://doi.org/10.1021/acs.nanolett.1c03703.

(2) Guo, X.; Xie, M.; Addhya, A.; Linder, A.; Zvi, U.; Deshmukh, T. D.; Liu, Y.; Hammock, I. N.; Li, Z.; DeVault, C. T.; Butcher, A.; Esser-Kahn, A. P.; Awschalom, D. D.; Delegan, N.; Maurer, P. C.; Heremans, F. J.; High, A. A. Direct-Bonded Diamond Membranes for Heterogeneous Quantum and Electronic Technologies. arXiv June 7, 2023. https://doi.org/10.48550/arXiv.2306.04408.

(3) Chen, H.; Asif, S.; Whalen, M.; Támara-Isaza, J.; Luetke, B.; Wang, Y.; Wang, X.; Ayako, M.; Lamsal, S.; May, A. F.; McGuire, M. A.; Chakraborty, C.; Xiao, J. Q.; Ku, M. J. H. Revealing Room Temperature Ferromagnetism in Exfoliated Fe5GeTe2 Flakes with Quantum Magnetic Imaging. *2D Mater.* **2022**, *9* (2), 025017. https://doi.org/10.1088/2053-1583/ac57a9.

(4) Chen, H.; Asif, S.; Dolui, K.; Wang, Y.; Támara-Isaza, J.; Goli, V. M. L. D. P.; Whalen, M.; Wang, X.; Chen, Z.; Zhang, H.; Liu, K.; Jariwala, D.; Jungfleisch, M. B.; Chakraborty, C.; May, A. F.; McGuire, M. A.; Nikolic, B. K.; Xiao, J. Q.; Ku, M. J. H. Above-Room-Temperature Ferromagnetism in Thin van Der Waals Flakes of Cobalt-Substituted Fe5GeTe2. *ACS Appl. Mater. Interfaces* **2023**, *15* (2), 3287–3296. https://doi.org/10.1021/acsami.2c18028.

(5) Marshall, M. C.; Ebadi, R.; Hart, C.; Turner, M. J.; Ku, M. J. H.; Phillips, D. F.; Walsworth, R. L. High-Precision Mapping of Diamond Crystal Strain Using Quantum Interferometry. *Phys. Rev. Appl.* **2022**, *17* (2), 024041. https://doi.org/10.1103/PhysRevApplied.17.024041.

(6) Broadway, D. A.; Johnson, B. C.; Barson, M. S. J.; Lillie, S. E.; Dontschuk, N.; McCloskey, D. J.; Tsai, A.; Teraji, T.; Simpson, D. A.; Stacey, A.; McCallum, J. C.; Bradby, J. E.; Doherty, M. W.; Hollenberg, L. C. L.; Tetienne, J.-P. Microscopic Imaging of the Stress Tensor in Diamond Using in Situ Quantum Sensors. *Nano Lett.* **2019**, *19* (7), 4543–4550. https://doi.org/10.1021/acs.nanolett.9b01402.

(7) Kehayias, P.; Turner, M. J.; Trubko, R.; Schloss, J. M.; Hart, C. A.; Wesson, M.; Glenn, D. R.; Walsworth, R. L. Imaging Crystal Stress in Diamond Using Ensembles of Nitrogen-Vacancy Centers. *Phys. Rev. B* **2019**, *100* (17), 174103. https://doi.org/10.1103/PhysRevB.100.174103.

(8) Marshall, M. C.; Turner, M. J.; Ku, M. J. H.; Phillips, D. F.; Walsworth, R. L. Directional Detection of Dark Matter with Diamond. *Quantum Sci. Technol.* **2021**, *6* (2), 024011. https://doi.org/10.1088/2058-9565/abe5ed.

(9) Ghiasi, T. S.; Borst, M.; Kurdi, S.; Simon, B. G.; Bertelli, I.; Boix-Constant, C.; Mañas-Valero, S.; van der Zant, H. S. J.; van der Sar, T. Nitrogen-Vacancy Magnetometry of CrSBr by Diamond Membrane Transfer. arXiv July 3, 2023. https://doi.org/10.48550/arXiv.2307.01129.